Article:
Liu, Q, Zuo, J, Zhu, C et al. (3 more authors) (2022) Design and Hierarchical Force-Position Control of Redundant Pneumatic Muscles-Cable-Driven Ankle Rehabilitation Robot. IEEE Robotics and Automation Letters, 7 (1). pp. 502-509. ISSN 2377-3766

https://doi.org/10.1109/lra.2021.3123747

Design and Hierarchical Force-Position Control of Redundant Pneumatic Muscles-Cable-Driven Ankle Rehabilitation Robot

Quan Liu, *Member, IEEE*, Jie Zuo, Chengxiang Zhu, Wei Meng, *Member, IEEE*, Qingsong Ai, *Member, IEEE*, Sheng Q. Xie, *Senior Member, IEEE*

***Abstract*—Ankle dysfunction is common in the public following injuries, especially for stroke patients. Most of the current robotic ankle rehabilitation devices are driven by rigid actuators and have problems such as limited degrees of freedom, lack of safety and compliance, and poor flexibility. In this paper, we design a new type of compliant ankle rehabilitation robot redundantly driven by pneumatic muscles (PMs) and cables to provide full range of motion and torque ability for the human ankle with enhanced safety and adaptability, attributing to the PM's high power/mass ratio, good flexibility and lightweight advantages. The ankle joint can be compliantly driven by the robot with full three degrees of freedom to perform the dorsiflexion/plantarflexion, inversion/ eversion, and adduction/abduction training. In order to keep all PMs and cables in tension which is essential to ensure the robot's controllability and patient's safety, Karush-Kuhn-Tucker (KKT) theorem and analytic-iterative algorithm are utilized to realize a hierarchical force-position control (HFPC) scheme with optimal force distribution for the redundant compliant robot. Experiment results demonstrate that all PMs are kept in tension during the control while the position tracking accuracy of the robot is acceptable, which ensures controllability and stability throughout the compliant robot-assisted rehabilitation training.**

***Index Terms*—Redundant robots, force control, pneumatic muscles, ankle rehabilitation robot.**

I. Introduction

ACCORDING to the Global Stroke Statistics in 2019, the mean global lifetime risk of stroke increased to 24.9% [1], while the data of China is up to 39.3%, which is the highest worldwide [2]. Most stroke patients will develop ankle dysfunction with persistent symptoms of ankle joint instability, foot drop and abnormal gait [3]. Ankle sprains also involve overstretching the ligaments and soft tissues around the ankle, are a common type of ankle injuries. In the UK, for example, there are over 2 million emergency department visits with sprained ankles a year, accounting for 5,600 incidences per day [4]. Up to 70% of people who incur a "simple" ankle sprain will develop a chronic ankle instability with decreased function and ankle joint instability [5]. The ankle dysfunction could impose huge indirect costs or tremendous economic burden on the society, e.g. costs of travel, productivity loss and care [4].

Traditional ankle treatment relies on therapists' one-to-one assisted therapy and rehabilitation. Due to the limited resources available in the hospitals or rehabilitation centers, robotics, as an alternative solution to perform general rehabilitation tasks, has shown great potential in the past decade [6]. Compared with traditional rigid actuators, soft actuators like pneumatic muscles (PMs) possess better flexibility and are more appropriate for human-robot interactions [7]. Thus far, there have been some preliminary robot prototypes for ankle rehabilitation, among which Stewart platform is one of the main types. It is more suitable for the joint with multiple degrees of freedom (DOFs) compared to the antagonistic configuration [8]. Jamwal *et al.* designed a 3-DOF ankle rehabilitation robot driven by PMs and cables [9]. Zhang *et al.* also developed a 3-DOF PM-driven ankle rehabilitation robot CARR [10]. These prototypes have difficulties in providing sufficient forces in the adduction/ abduction movement, unable to satisfy the ankle rehabilitation needs in some DOFs [11]. Tu *et al.* introduced functional electrical stimulation (FES) to supplement the exoskeleton's assistance for ankle joint [12]. Krishnan *et al.* proposed a parallel PM-driven ankle rehabilitation robot (ARR) with the top moving platform supported by a central strut between the top and the bottom [13]. Though this robot covers the 3-DOF movement range, it is difficult to provide effective assistance for patients due to a lack of rigid connection to the lower limb [11]. Since PMs only generate pulling force rather than pushing force, PM-driven robots should be designed in redundant configuration to close the force loop [9, 14, 15]. To achieve n DOFs of movement, at least $n+1$ PMs must be applied [16].

As the driving characteristics of PMs are similar to cables, if a certain PM's expected driving force calculated from dynamics is negative, that is, the PM is in a relaxed state. Then the PM-actuated rehabilitation robot will lose its control, which might bring secondary injuries to patients [17]. In order to ensure the robot's controllability and the patient's safety during the robot-assisted rehabilitation, it is essential to keep all PMs in the state of tension throughout the training process. However, a pure position controller can only enable the robot to follow an expected trajectory, but cannot ensure that each PM is always in tension. Moreover, the PM's compliant features could bring patients a certain range of arbitrary movement which may lead to a risk of deviation from the safe workspace, especially for patients with muscle atrophy or spasms. Existing methods mainly focus on PM's position control with little consideration on the force control [18]. Jouppila *et al.* proposed an integrated sliding mode controller (SMC) [19], and an adaptive back stepping sliding mode controller was proposed for a 2-DOF PM-driven robot [20] to solve the human-robot uncertainties. Only a few existing studies focus on force/torque distribution, but mainly aimed at

minimizing the energy consumption or the motor size [21, 22]. To achieve the minimum of the total driving forces, Su *et al.* transformed the force optimization into a convex programming problem and solved it using polynomial optimization approach [23]. Mao *et al.* optimized the tensioned workspace for an anthropomorphic arm exoskeleton CAREX [24]. Jin *et al.* utilized a force field controller for the C-ALEX exoskeleton to provide low-cost assistance [25]. To optimize C-ALEX's force for post-stroke participants, Hidayah *et al.* evaluated the cable's force out of the plane movements relative to the desired tension magnitudes [26]. Hassan *et al.* proposed a projection-based force distribution method for a 3-DOF parallel manipulator [27]. Yuan *et al.* developed a force distribution method considering the rope sag effect with an optimization scheme and a user-defined cost function to ensure the positive driving forces [28]. Existing references mostly focus on low-cost force assistance and energy saving for devices with rigid actuators. Only a few studies proposed force distribution methods, but cannot satisfy the force control needs of soft actuators in robot-assisted rehabilitation, not considering the distributed driving forces' lower limit, as well as their real-time solutions. Furthermore, though the redundant PM-driven configuration can effectively avoid the singularities of the parallel mechanism in the working space, but also leads to the innumerable solutions of driving force distribution. However, these limitations cannot be ignored in practice, since the clinical rehabilitation ask for high safety and controllability towards patients.

The study on optimal force control of PM-driven redundant robot is limited. Most of the studies with PMs using McKibben actuators just tried to do simple assist flexion/extension rather than full joint movement control. In this paper, we design a hierarchical force-position controller (HFPC) with optimal force distribution by redistributing the expected driving forces of PMs to guarantee their tension states. Main contributions of this work include: 1) designing and modelling a new compliant ankle rehabilitation robot redundantly driven by PMs and cables, to cover full motion and force range for human ankle joint with enhanced safety and adaptability; 2) proposing an optimal force distribution method based on Karush-Kuhn-Tucker (KKT) theorem and analytic-iterative algorithm on a redundant PM-driven rehabilitation robot; and 3) designing a hierarchical force-position control scheme to ensure all PMs are in tension for enhanced training safety and reasonable trajectory tracking accuracy. The rest of this paper is organized as follows: Section II describes the design and modelling of the PM-cable-driven ankle rehabilitation robot, followed by the optimal force distribution based hierarchical force-position controller in Section III. Experimental analysis of a series of feasibility tests for the robot and controller with/without human participants are presented in Section IV, and Section V concludes the paper.

II. Design and Modelling of the Compliant Ankle Rehabilitation Robot

A. PMs-Cable-Driven Robot Design

With three rotational DOFs, the ankle is one of the most complex and vulnerable joints of human body. As shown in Fig. 1, the ankle rehabilitation robot mainly includes three parts: moving module, PM-driven module and support module. The moving platform is mainly composed of rotating joint 1/2/3 around the *X*/*Y*/*Z* axes and their support rods. The PM-driven module is shown in Fig. 2, mainly including five PMs, fixed/ swinging pulleys and their support. Each PM is connected to the moving platform's fixed point with the cable through the pulley. PM 1 and PM 2 actuate the moving platform to perform inversion/eversion (around *Y*-axis); PM 3 and PM 4 drive the moving platform to do adduction/abduction (around *Z*-axis); PM 5 is connected to the fixed point at the moving platform's back end, working with PM 1 and PM 2 to help ankle perform dorsiflexion/plantarflexion (around *X*-axis). More details have been presented in our previous research paper [29].

The whole 3-DOF PM-driven ankle rehabilitation robot was developed, as shown in Fig. 3. The robot is actuated by five PMs (DMSP-20-400N, Festo, Germany), the air pressure inside each PM is controlled by a proportional valve regulator (VPPM-6L-L-1-G18-0L6H, Festo, Germany). The displacement of each PM is measured by a rope displacement sensor (MPS-XXXS-200mm-V2, Miran Technology, China) and its driving force is measured by a force sensor (DJYZ-25-100Kg, DJsensor, China). Three rotational joints of the moving platform correspond to three axes, i.e., *X*-, *Y*- and *Z*- axis. Each rotation joint is equipped with a magnetic angle sensor (EVB-MLX90316GO, Melexis, Belgium) to measure the robot's rotation angles. In order to obtain the interaction torque between the patient's ankle and the robot, a six-axis force/torque sensor (M3715A, SRI, China) is fixed between the footboard and the robot end-effector.

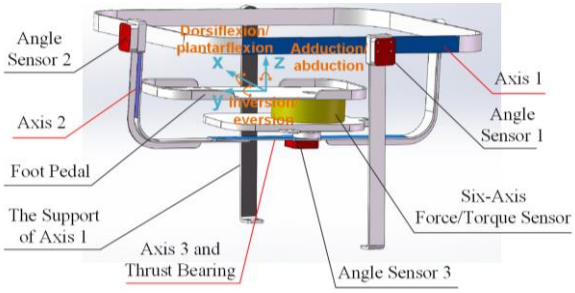

Fig. 1. Design of the robot moving platform.

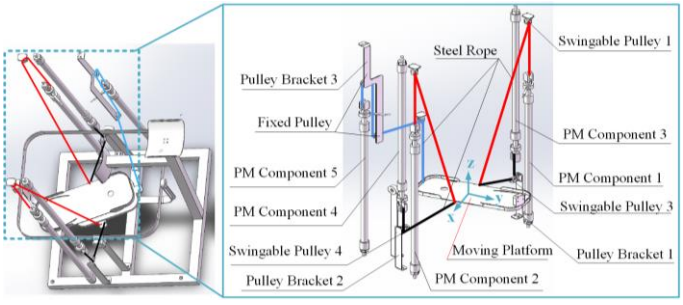

Fig. 2. Design of the robot driving modules.

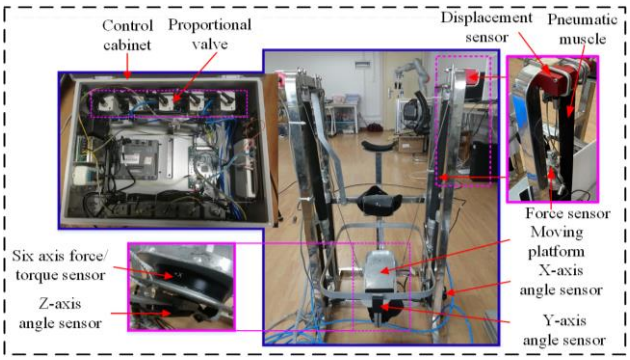

Fig. 3. The developed compliant ankle rehabilitation robot redundantly driven by PMs and cables.

B. Kinematics Modelling

To realize the position and force control for the developed robot, it is essential to establish its inverse kinematic model, dynamic model and Jacobian matrix of the robot. Based on the robot's geometric model in Fig. 4, the coordinate system of the fixed platform and moving platform are defined as $O_f - XYZ$ and $O_m - XYZ$, while $O_R - XYZ$ is the moving platform's rotating coordinate system. The i-th $(i = 1,2,\cdots,5)$ connection point of the cable with the fixed platform is P_i^f, and its i-th connection point with the moving platform is P_i^m. O_f and O_m are the fixed platform center and the moving platform center, respectively; while O_R is the moving platform's actual rotating center. The rotation angle vector of the moving platform is $\boldsymbol{q} = [\theta_x\,;\theta_y\,;\theta_z]$, where θ_x, θ_y and θ_z are rotation angles around the X-, Y- and Z-axis, respectively. The vector from the connection point P_i^f to P_i^m, i.e., the instantaneous cable length, can be expressed as (1). $\boldsymbol{R} = \boldsymbol{R}_z\boldsymbol{R}_y\boldsymbol{R}_x$ denotes the moving platform's rotation matrix, where $\boldsymbol{R_x}$, $\boldsymbol{R_y}$ and $\boldsymbol{R}_z$ are corresponding rotation matrix around the X-, Y- and Z-axis.

$$\boldsymbol{L}_i = \overrightarrow{O_fO_R} + \boldsymbol{R}\overrightarrow{O_RP_i^m} - \overrightarrow{O_fP_i^f} \tag{1}$$

Then the displacement change of each PM link is:

$$\Delta l_i = \|\boldsymbol{L}_i\| - l_{i0} = \left\|\overrightarrow{O_fO_R} + \boldsymbol{R}\overrightarrow{O_RP_i^m} - \overrightarrow{O_fP_i^f}\right\| - l_{i0} \tag{2}$$

where l_{i0} is the initial length of the i-th link.

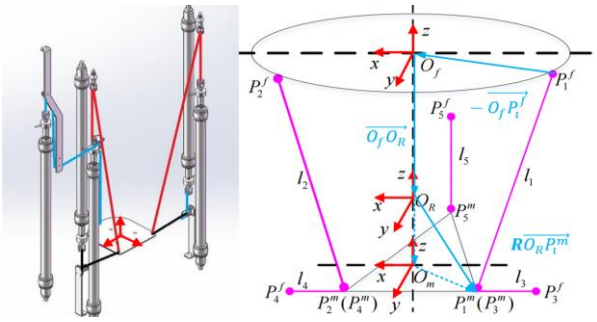

Fig. 4. Mechanism and geometric model of the ankle robot.

C. Dynamics Modelling

The dynamic model of the moving platform can be expressed in the form of (3). $\dot{\boldsymbol{q}}$ and $\ddot{\boldsymbol{q}}$ are the first and the second derivatives of the robot's rotation angle with respect to time. $\boldsymbol{M}(\boldsymbol{q})$, $\boldsymbol{C}(\boldsymbol{q},\dot{\boldsymbol{q}})$ and $\boldsymbol{G}(\boldsymbol{q})$ denote the inertia matrix, the Coriolis force matrix and gravity of the moving platform, respectively. Thus the robot's desired output torque $\boldsymbol{\tau}$ is:

$$\boldsymbol{\tau} = \boldsymbol{M}(\boldsymbol{q})\ddot{\boldsymbol{q}} + \boldsymbol{C}(\boldsymbol{q},\dot{\boldsymbol{q}})\dot{\boldsymbol{q}} + \boldsymbol{G}(\boldsymbol{q}) \tag{3}$$

The simulation was conducted to evaluate the robot model and verify its movement ability, as shown in Fig. 5. The robot's moving platform was controlled to track a predefined trajectory. Since PMs can only provide pulling force, the negative value may cause the robot out of control. Thus the PM's driving force need to be redistributed to ensure its tension state for the PM-driven robot's controllability in practice.

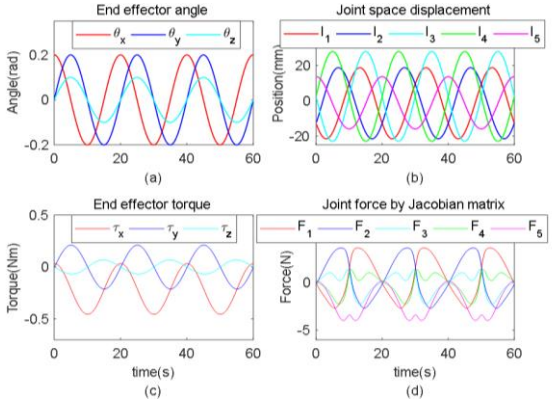

Fig. 5. Kinematic and dynamic modelling simulation results of the robot. (a) The trajectory of the moving platform; (b) The displacement changes of all PMs; (c) The torque required to drive the moving platform; (d) The required PM driving forces.

III. Optimal Force Distribution Based Hierarchical Force-Position Control

An optimal force distribution method with Karush-Kuhn-Tucker (KKT) theorem and analytic-iterative algorithm is proposed on the basis of studies [30, 31], to obtain the optimal force distribution constraint equations. An iterative search algorithm is applied to find out the appropriate solution with the minimum driving force greater than a certain value.

A. KKT-Based Force Distribution

Since the 3-DOF ankle rehabilitation robot is redundantly driven by five PMs, there are innumerable combinations of torques $\boldsymbol{\tau}_{m\times1}(m=3)$ and joint driving forces $\boldsymbol{F}_{n\times1}(n=5)$ for the robot's movement. Jacobian matrix $\boldsymbol{J}$ describes the relationship between the PM's speed and the moving platform's end angle, as well as the relationship between $\boldsymbol{\tau}_{m\times1}$ and $\boldsymbol{F}_{n\times1}$, i.e., $\boldsymbol{\tau}_{m\times1} = (\boldsymbol{J}^T)_{m\times n}\boldsymbol{F}_{n\times1}$. One of the solutions can be obtained by using (4) to determine the joint space driving force. To guarantee that the PM's driving force is always positive, the most critical problem is to choose the appropriate value for the element $\boldsymbol{y}$, so it can be regarded as an optimization problem.

$$\boldsymbol{F}_{n\times1} = \boldsymbol{F}_0 + \boldsymbol{A}\boldsymbol{y} \tag{4}$$

where $\boldsymbol{F}_0$ are original driving forces calculated from the robot dynamics by $\boldsymbol{F}_0 = \boldsymbol{J}^{T+}\boldsymbol{\tau}_{m\times1}$, in which $\boldsymbol{J}^{T+} = \boldsymbol{J}(\boldsymbol{J}^T\boldsymbol{J})^{-1}$, and the value of $\boldsymbol{F}_0$ may be negative as shown in Fig. 5 (d). To ensure the value of actual driving forces $\boldsymbol{F}_{n\times1}$ are always greater than the set minimum positive value, $\boldsymbol{A}\boldsymbol{y}$ is added as the forces for compensation. $\boldsymbol{A} = orthonormal\{\boldsymbol{I}_{n\times n} - \boldsymbol{J}^{T+}\boldsymbol{J}^T\}$ denotes an orthogonal matrix, $\boldsymbol{I}_{n\times n}$ is an identity matrix. $\boldsymbol{y}$ can be regarded as the compensating forces to be resolved. By choosing an appropriate $\boldsymbol{y}$, each element of $\boldsymbol{F}_{n\times1}$ is greater than the set value and satisfies $\boldsymbol{\tau}_{m\times1} = (\boldsymbol{J}^T)_{m\times n}\boldsymbol{F}_{n\times1}$ when minimizing the total driving force, thus the PM driving forces meet the minimum tension needs. The problem can be regarded as an optimization problem with equality and inequality constraints. The objective function of the optimization problem is expressed by (5).

$$\min_{\boldsymbol{y}} f(\boldsymbol{y}) = (\boldsymbol{F}_0 + \boldsymbol{A}\boldsymbol{y})^T(\boldsymbol{F}_0 + \boldsymbol{A}\boldsymbol{y}) \tag{5}$$

$$\begin{cases} g(\boldsymbol{y}) = \boldsymbol{\tau}_{m\times1} - (\boldsymbol{J}^T)_{m\times n}(\boldsymbol{F}_0 + \boldsymbol{A}\boldsymbol{y}) = 0 \\ r(\boldsymbol{y}) = \boldsymbol{F}_{\min} - (\boldsymbol{F}_0 + \boldsymbol{A}\boldsymbol{y}) \le 0 \end{cases} \tag{6}$$

where $g(\boldsymbol{y})$ and $r(\boldsymbol{y})$ are the constrain conditions of (5). $\boldsymbol{F}_{\min}$ is a vector with all elements greater than a certain positive value, and in this case all PMs are in tension. To find out the optimal solution that satisfies the constraint, KKT theorem was utilized to solve the problem by defining the Lagrangian function as:

$$\varepsilon(\boldsymbol{y}, \boldsymbol{\lambda}, \boldsymbol{\mu}) = f(\boldsymbol{y}) + \boldsymbol{\lambda}^T g(\boldsymbol{y}) + \boldsymbol{\mu}^T r(\boldsymbol{y}) \tag{7}$$

$\boldsymbol{\lambda} = [\lambda_1, \lambda_2, \cdots, \lambda_m]^T$ and $\boldsymbol{\mu} = [\mu_1, \mu_2, \cdots, \mu_n]^T$ are Lagrangian multipliers. According to the KKT theorem, if (8) and (9) are satisfied under conditions of $g(\boldsymbol{y}) = 0$, $r(\boldsymbol{y}) \le 0$, and $\boldsymbol{\mu}^0 = [\mu_1^0, \mu_2^0, \cdots, \mu_n^0], \mu_i^0 \ge 0$, $\boldsymbol{y} = \boldsymbol{y}_0$ is the optimal solution of $f(\boldsymbol{y})$.

$$\frac{\partial}{\partial \boldsymbol{y}}(\boldsymbol{y}, \boldsymbol{\lambda}, \mu)|_{\substack{\boldsymbol{y}=\boldsymbol{y}_0 \\ \boldsymbol{\lambda}=\boldsymbol{\lambda}_0 \\ \boldsymbol{\mu}=\boldsymbol{\mu}_0}} = \frac{\partial}{\partial \boldsymbol{y}}(f(\boldsymbol{y}) + \boldsymbol{\lambda}^T g(\boldsymbol{y}) + \boldsymbol{\mu}^T r(\boldsymbol{y}))_{\substack{\boldsymbol{y}=\boldsymbol{y}_0 \\ \boldsymbol{\lambda}=\boldsymbol{\lambda}_0 \\ \boldsymbol{\mu}=\boldsymbol{\mu}_0}} = 0 \tag{8}$$

In addition, the optimal solution $\boldsymbol{y}_0$ meets the condition:

$$\boldsymbol{\mu}^T r(\boldsymbol{y})|_{\boldsymbol{y}=\boldsymbol{y}_0} = 0 \tag{9}$$

Combining (5)-(7) and (9), the constraint equations are:

$$\begin{cases} 2\boldsymbol{A}^T\boldsymbol{F}_0 + 2\boldsymbol{y}_0 - \boldsymbol{A}^T\boldsymbol{J}\boldsymbol{\lambda} - \boldsymbol{A}^T\boldsymbol{\mu} = 0 \\ \boldsymbol{\tau}_{m\times1} - (\boldsymbol{J}^T)_{m\times n}(\boldsymbol{F}_0 + \boldsymbol{A}\boldsymbol{y}_0) = 0 \\ \boldsymbol{\mu}^T(\boldsymbol{F}_{\min} - \boldsymbol{F}_0 - \boldsymbol{A}\boldsymbol{y}_0) = 0 \end{cases} \tag{10}$$

B. Analytical Solutions

Since $\mu_i \ge 0$ and $r_i(\boldsymbol{y}_0) \le 0$, (9) can be written as:

$$\begin{cases} \mu_i = 0 & for \quad r_i(\boldsymbol{y}_0) < 0 \\ \mu_i \ge 0 & for \quad r_i(\boldsymbol{y}_0) = 0 \end{cases} \tag{11}$$

According to $r_i(\boldsymbol{y}_0) = (\boldsymbol{F}_{\min})_i - (\boldsymbol{F}_{n\times1})_i = 0$ or < 0, the solution to the optimization problem can be divided into the following three cases, namely:

Case1: All driving forces are located at the boundary of the feasible domain defined by the inequality constraint;

Case2: All driving forces are inside the feasible domain defined by the inequality constraint;

Case3: Some of the driving forces lie on the boundary of the feasible domain, while others lie inside the feasible domain.

For the case demonstrated in **Case1**, $r_i(\boldsymbol{y}_0) = 0$ is satisfied, so the optimal driving force can be obtained by (12).

$$\boldsymbol{F}_{n\times1} = \boldsymbol{F}_0 + \boldsymbol{A}\boldsymbol{y}_0 = \boldsymbol{F}_{\min} \tag{12}$$

For **Case2**, $\mu_i = 0$ and $r_i(\boldsymbol{y}_0) < 0$ are always satisfied. So (10) can be converted into:

$$\begin{cases} -2\boldsymbol{y}_0 + \boldsymbol{A}^T\boldsymbol{J}\boldsymbol{\lambda} = 2\boldsymbol{A}^T\boldsymbol{F}_0 \\ (\boldsymbol{J}^T)_{m\times n}\boldsymbol{A}\boldsymbol{y}_0 = \boldsymbol{\tau}_{m\times1} - (\boldsymbol{J}^T)_{m\times n}\boldsymbol{F}_0 \end{cases} \tag{13}$$

Thus, $\boldsymbol{y}_0$ can be solved by (14):

$$\begin{cases} [\boldsymbol{B}_0]_{(n+m)\times(n+m)} \cdot [\boldsymbol{X}_0]_{(n+m)\times1} = [\boldsymbol{C}_0]_{(n+m)\times1} \\ [\boldsymbol{X}_0]_{(n+m)\times1} = ([\boldsymbol{B}_0]_{(n+m)\times(n+m)})^{-1} \cdot [\boldsymbol{C}_0]_{(n+m)\times1} \end{cases} \tag{14}$$

where

$$\boldsymbol{B}_0 = \begin{bmatrix} -2\boldsymbol{I}_{n\times n} & [\boldsymbol{A}^T\boldsymbol{J}]_{n\times m} \\ [\boldsymbol{J}^T\boldsymbol{A}]_{m\times n} & 0_{m\times m} \end{bmatrix}; \boldsymbol{X}_0 = \begin{bmatrix} (\boldsymbol{y}_0)_{n\times1} \\ \boldsymbol{\lambda}_{m\times1} \end{bmatrix};$$
$$\boldsymbol{C}_0 = \begin{bmatrix} [2\boldsymbol{A}^T\boldsymbol{F}_0]_{n\times1} \\ [\boldsymbol{\tau}_{m\times1} - \boldsymbol{J}^T\boldsymbol{F}_0]_{m\times1} \end{bmatrix} \tag{15}$$

The value of $\boldsymbol{y}_0$ can be obtained by (14) and (15), so

$$\boldsymbol{F}_{n\times1} = \boldsymbol{F}_0 + \boldsymbol{A}\boldsymbol{y}_0 = \boldsymbol{F}_0 + \boldsymbol{A}\boldsymbol{X}_0(1:n) \tag{16}$$

For **Case3**, assume that there are $S(1 \le S < n)$ actuators whose driving forces locate at the boundary of the feasible domain defined by the inequality constraint. For $i \in [1,2,\cdots,n]$, $r_i(\boldsymbol{y}_0) = 0$ and $\mu_i \ge 0$, $\boldsymbol{F}_i = (\boldsymbol{F}_{\min})_i$. The driving forces of the remaining $n - S$ actuators are inside the feasible domain, i.e., for $j \in [1,2,\cdots,n]$ and $j \ne i$, $r_j(\boldsymbol{y}_0) < 0$ and $\mu_j = 0$.

Thus, $\boldsymbol{y}_0$ can be obtained by (17).

$$\begin{cases} [\boldsymbol{B}]_{(n+m+n_i)\times(n+m+n_i)} \cdot [\boldsymbol{X}]_{(n+m+n_i)\times1} = [\boldsymbol{C}]_{(n+m+n_i)\times1} \\ [\boldsymbol{X}]_{(n+m+n_i)\times1} = [\boldsymbol{B}^{-1}]_{(n+m+n_i)\times(n+m+n_i)} \cdot [\boldsymbol{C}]_{(n+m+n_i)\times1} \end{cases} \tag{17}$$

where

$$\boldsymbol{B} = \begin{bmatrix} [\boldsymbol{B}_0]_{(n+m)\times(n+m)} & \begin{bmatrix} [\vec{a}_1^T, \cdots, \vec{a}_i^T]_{n\times n_i} \\ 0_{m\times n_i} \end{bmatrix} \\ \begin{bmatrix} \begin{bmatrix} \vec{a}_1 \\ \vdots \\ \vec{a}_i \end{bmatrix}_{n_i\times n} & 0_{n_i\times m} \end{bmatrix} & 0_{n_i\times n_i} \end{bmatrix};$$
$$\boldsymbol{X} = \begin{bmatrix} (\boldsymbol{y}_0)_{n\times1} \\ \boldsymbol{\lambda}_{m\times1} \\ \begin{bmatrix} \mu_1 \\ \vdots \\ \mu_i \end{bmatrix} \end{bmatrix}; \boldsymbol{C} = \begin{bmatrix} 2\boldsymbol{A}^T\boldsymbol{F}_0 \\ \boldsymbol{\tau}_{m\times1} - \boldsymbol{J}^T\boldsymbol{F}_0 \\ \begin{bmatrix} \boldsymbol{F}_{\min_1} - \boldsymbol{F}_{0_1} \\ \vdots \\ \boldsymbol{F}_{\min_i} - \boldsymbol{F}_{0_i} \end{bmatrix} \end{bmatrix} \tag{18}$$

where $n_i(1 \le n_i < n)$ is the total number of cases when $r_i(\boldsymbol{y}_0) = 0$. Let $\boldsymbol{A} = [\overrightarrow{a_1}; \cdots; \overrightarrow{a_n}]$ and for each case $r_i(\boldsymbol{y}_0) = 0$, $\overrightarrow{a_i}$ is the corresponding row vector of matrix $\boldsymbol{A}$. u_i, $\boldsymbol{F}_{\min_i}$ and $\boldsymbol{F}_{0_i}$ are corresponding values in the respective vectors. So:

$$\boldsymbol{F}_{n\times1} = \boldsymbol{F}_0 + \boldsymbol{A}\boldsymbol{y}_0 = \boldsymbol{F}_0 + \boldsymbol{A}\boldsymbol{X}_0(1:n) \tag{19}$$

C. Iterative Search Algorithm for Optimal Solution

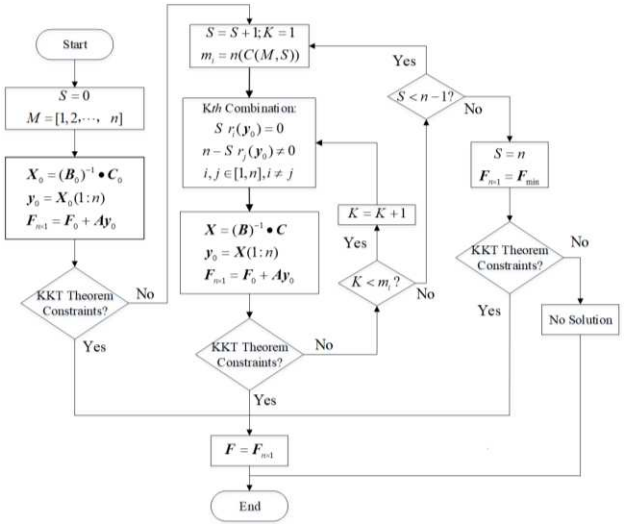

Fig. 6. Flow chart of the iterative search algorithm for the optimal force distribution solution of the redundant robot.

The iterative search algorithm was designed to find out the optimal solution for the force distribution, with detailed steps shown in Fig. 6. In the first iteration loop, assume that all driving forces are within the feasible domain defined by the inequality constraints. That is, corresponding to **Case2**, if $\boldsymbol{F}_{n\times1}$ satisfies the constraint condition of the KKT theorem, the algorithm terminates and $\boldsymbol{F}_{n\times1}$ is the optimal solution. Otherwise, there is a combination of forces on the boundary of the feasible domain. For $\boldsymbol{M} = [1,2,\cdots,n]^T$ of all driving forces, there are $S(1 \le S < n)$ forces at the boundary of the feasible domain. $\boldsymbol{C}(\boldsymbol{M}, S)$ denotes a combination of $\boldsymbol{M}$ and S. By changing the value of S in the iterative loop, all possible combinations are examined. This assumption is the same as **Case3**. The algorithm terminates if $\boldsymbol{F}_{n\times1}$ satisfies the constraints of the KKT theorem and $\boldsymbol{F}_{n\times1}$ is the resulted optimal solution. The last loop of the iterative search algorithm is actually similar to **Case1**. All driving forces are on the boundary of the feasible domain, i.e., $\boldsymbol{F}_{n\times1} = \boldsymbol{F}_{\min}$. If the constraint of KKT theorem is satisfied, $\boldsymbol{F}_{n\times1}$ is the optimal solution. Otherwise, the constraint equation has no solution.

D. Simulation validation

In order to verify the performance of the proposed force distribution method, simulation tests were carried out and the robot's desired trajectory was set as (20).

$$\begin{cases} \boldsymbol{q} = [\theta_x;\theta_y;\theta_z] = [36/\pi * cos\omega t; 27/\pi * sin\,\omega t; 18/\pi * sin\,\omega t](°) \\ \boldsymbol{\tau}_r = [\tau_x;\tau_y;\tau_z] = \boldsymbol{M}(\boldsymbol{q})\ddot{\boldsymbol{q}} + \boldsymbol{C}(\boldsymbol{q},\dot{\boldsymbol{q}})\dot{\boldsymbol{q}} + \boldsymbol{G}(\boldsymbol{q}) \\ \boldsymbol{\tau}_{total} = \boldsymbol{\tau}_r + \boldsymbol{\tau}_{int}; \boldsymbol{\tau}_{int} = [-0.01 * t; 0; 0]; \\ f = 0.05,\ \ \omega = 2\pi f \end{cases} \tag{20}$$

Based on the kinematic model and the desired trajectory, $\boldsymbol{\tau}_r$ to be overcome is calculated, and the external torque applied to the robot is denoted by $\boldsymbol{\tau}_{int}$, thus the total torque that robot has to overcome is $\boldsymbol{\tau}_{total} = \boldsymbol{\tau}_r + \boldsymbol{\tau}_{int}$. Based on the force distribution method, an optimal result is obtained according to the set minimum driving force, ensuring that all PMs are generating pulling forces. Define the driving forces $\boldsymbol{F} = [F_1;F_2;F_3;F_4;F_5]$ and the Jacobian matrix $\boldsymbol{J}$, and the robot's calculated torque $\boldsymbol{\tau}_{fd}$ could be calculated through forward dynamics. If $\boldsymbol{\tau}_{fd}$ is equal to $\boldsymbol{\tau}_{total}$, the distributed forces enable robot to follow the desired trajectory, then the force distribution method is verified. Here the minimum driving force is set to 10 N, and the simulation results are presented in Fig. 7. It is clear that all driving forces in (c) are not less than 10N under the force distribution method and the torque recalculated by Jacobian matrix in (d) is consistent with the total torque robot needs to overcome in (b). Thus the simulation validates the force distribution method, which can drive the robot to achieve the desired movement and keep all PMs in tension.

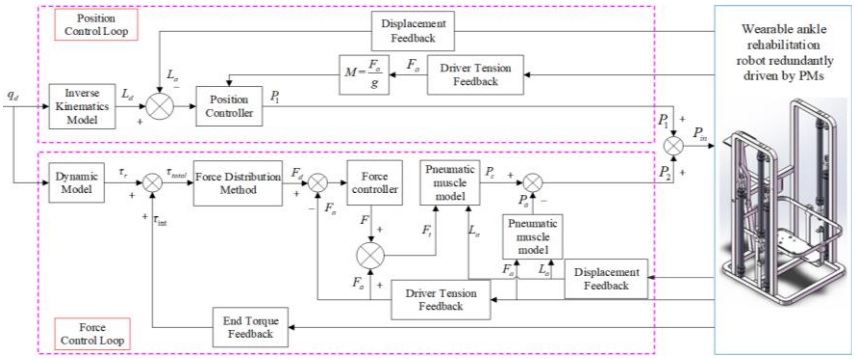

Fig. 8. The proposed hierarchical force-position control scheme based on optimal force distribution for the ankle rehabilitation robot.

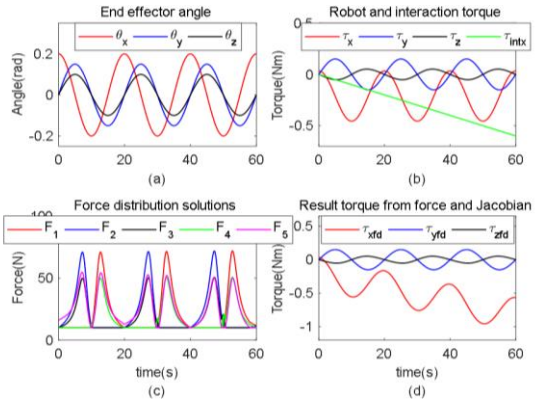

Fig. 7. Simulation results to validate the force distribution method with external torque. (a) The desired trajectory of the robot; (b) The torque calculated by the dynamic model and the assumed external torque; (c) Each PM's driving force based on optimal force distribution; (d) The recalculated robot torque.

E. Hierarchical Force-Position Control (HFPC)

With the optimal force distribution, the ankle rehabilitation robot could be controlled in both position and force domains. A hierarchical force-position controller (HFPC) including a position control loop and a force control loop is proposed. The

position control loop is compensated by the force control loop with optimal force distribution. Such a control scheme enables the redundant robot to perform the desired tasks with all PMs in tension. As shown in Fig. 8, in terms of trajectory tracking control in the position control loop, an adaptive backstepping sliding mode controller (ABS-SMC) is employed to obtain the desired pressure P_1 of each PM, which has been presented in our previous work [20]. In the force control loop, the required robot torque $\boldsymbol{\tau}_r$ is calculated through the robot's dynamic model with desired movement $\boldsymbol{q}_d$. The total torque to overcome is $\boldsymbol{\tau}_{total} = \boldsymbol{\tau}_r + \boldsymbol{\tau}_{int}$, where $\boldsymbol{\tau}_{int}$ is the measured interaction torque. The PM's desired driving force F_d is calculated by the force distribution method. Then, comparing the error between F_d and the measured PM force F_a, the adopted PID force controller can continuously generate the output F, which is added to F_a to get the updated desired force F_t. The required pressure P_c is obtained based on the PM model with F_t and actual displacement L_a. F_a and L_a are utilized to calculate the nominal pressure P_a. Combining with the output pressure from both position and force control loop, the final pressure is used to simultaneously control the trajectory and torque of the robot.

IV. Experiments and Results Discussion

To validate the performance of the proposed HFPC scheme, experiments with HFPC were conducted on the developed ankle rehabilitation robot, in comparison with a pure position controller ABS-SMC. The experiments were divided into two groups: (1) without subject; (2) involving subjects. All subjects were asked to place their right feet on the robot's moving platform. Robot-assisted rehabilitation training should be carried out following a low-speed reciprocating motion to ensure patient's movement safety. Here the robot's desired trajectory was set as $\theta_x = 36/\pi * cos(2\pi ft)$ (°), $\theta_y = 36/\pi * sin(2\pi ft)$ (°), $\theta_z = 18/\pi * sin(2\pi ft)$ (°), $f = 0.05Hz$.

A. Experiments without participants

Experiments without subjects were firstly conducted to confirm the basic control performance on the robot. Seen from Fig. 9 and Table I, though there are some deviations between the practical value and the desired value, all PMs are able to follow the desired pulling forces. The trajectory tracking results of ABS-SMC and HFPC are demonstrated in Fig. 10. HFPC's maximum errors (ME) in *X*- and *Y*-axis are less than 2.53°, and ME in *Z*-axis is less than 1.26°. HFPC's trajectory tracking performance is quite similar to ABS-SMC, with a slightly weaker accuracy. From Table II, AE in *X*-axis increases from 0.54° to 1.05° when HFPC is adopted with respect to the ABS-SMC without subjects participation. HFPC's trajectory tracking performance is deteriorated compared with pure position control, since the compensation from force loop may affect the position tracking. But the decline is reasonable because the priority in robot-assisted rehabilitation is to ensure the patient's safety and controllability, so it is acceptable to sacrifice a certain trajectory tracking accuracy to keep all PMs in tension.

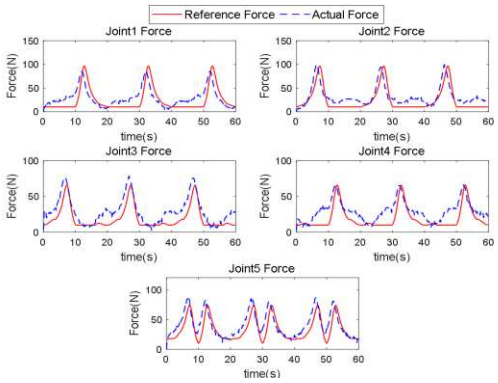

Fig. 9. Force tracking results of the ankle rehabilitation robot controlled by HFPC, in which the desired force is obtained by the optimal force distribution with the minimum force 10N.

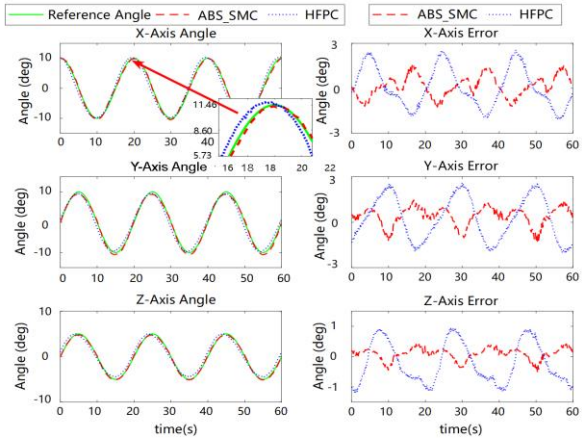

Fig. 10. Trajectory tracking results of the ankle rehabilitation robot controlled by ABS-SMC and HFPC without subjects.

TABLE I
STATISTICAL RESULTS OF THE FORCE TRACKING ERRORS IN JOINT SPACE UNDER HFPC CONTROL WITHOUT PARTICIPANTS

Error*	F1	F2	F3	F4	F5
AE (N)	15.018	13.098	10.617	11.477	10.940
RMSE (N)	17.649	15.284	12.937	13.772	14.175

*AE is average error, and RMSE is root mean square error.

TABLE II
STATISTICAL RESULTS OF TRAJECTORY TRACKING ERRORS UNDER TWO CONTROL METHODS WITHOUT SUBJECTS

Control method	AE (degrees)			RMSE (degrees)		
	X	*Y*	*Z*	*X*	*Y*	*Z*
ABS-SMC	0.54	0.62	0.21	0.67	0.69	0.25
HFPC	1.05	1.19	0.73	1.25	1.37	0.80

B. Experiments with Participants

For the alidation of HFPC's robustness for different users, experiments were conducted involving five healthy subjects, and their basic information is shown in Table III. This trial has been approved by Human Participants Ethics Committee from Wuhan University of Technology, and written informed consent was obtained from each participant. Due to the human interaction torque (Fig. 11), the desired driving forces obtained by HFPC (Fig. 12) are different from that without

subjects (Fig. 9). The result of subject 1 (S1) is taken as an example to analyze the control performance, as shown in Fig. 13. The robot still maintains a high trajectory tracking accuracy with subject's interaction. The ME in *X*- and *Y*-axis is less than 2.86°, while the ME in *Z*-axis is less than 1.61°. Thus, even with participants, the HFPC enables the ankle rehabilitation robot to assist them to perform accurate movement training.

Experimental results with five subjects are demonstrated in Tables IV and V to validate HFPC's performance (in which the underlined values are the highest values of F1/F2/F3/F4/F5 in the group of five subjects, respectively). Seen from Table IV, under the control of HFPC, five subjects' AE in three axes respectively increase by 54%, 59% and 76% compared with that of no participants. This is due to the human-robot interaction's negative effects on the robot's force-position control [32]. In [33], the average tracking errors remain the same (0.39 mm) for both load groups of 1 kg and 4.5 kg, but the mass is too small compared to the weight of human body. When the mass increases by 50 kg, the maximum tracking error increases by over 5 times [34]. Thus the decline of the proposed HFPC's tracking accuracy is satisfactorily acceptable with participants involved. Table V illustrates that HFPC achieves its main purpose of keeping each PM kept in tension even with participants. According to the results with five different users, HFPC is able to effectively maintain safety and controllability of the PM-driven ankle rehabilitation robot.

To further confirm the HFPC's tracking performance, a comparison is made with relevant studies of the pure position control for PM-driven devices [35-37] . Since the movement range and evaluation index in each reference are not exactly the same, they are normalized to the maximum error percentage in total movement range, with the detailed comparison results shown in Table VI. The performance of HFPC without subjects (22.07%) is just weaker than the robust iterative feedback tuning (IFT) controller in [35]. Even if HFPC's position control accuracy decreases with a subject's participation, the error of 28.09% is still better than that of [36, 37]. For robot-assisted rehabilitation, the safety of patients is the top priority in the training process. Due to the PM's compliant features, the PM-actuated robot has a certain space of arbitrary movement, which provides patients with compliant assistance, but also increases the risk of secondary injuries. Thus it is acceptable to sacrifice certain trajectory tracking accuracy to keep all PMs in tension. The proposed HFPC enables all PMs to be in tension to prevent the PM-actuated robot's deviation from the safe workspace, effectively reducing the risk of accidental injury. The HFPC's controllability is also acceptable in trajectory tracking even compared with some pure position controllers [35-37]. With the advantages of enhanced training safety and reasonable tracking accuracy, HFPC makes the PM-driven soft rehabilitation robot more suitable and practical in actual clinical conditions.

TABLE III
INFORMATION OF THE PARTICIPATED HEALTHY SUBJECTS

Subjects	Gender	Age	Height (cm)	Weight(kg)
S1	Male	25	176	68
S2	Male	24	175	65
S3	Female	24	160	51
S4	Female	25	163	50
S5	Male	25	178	70

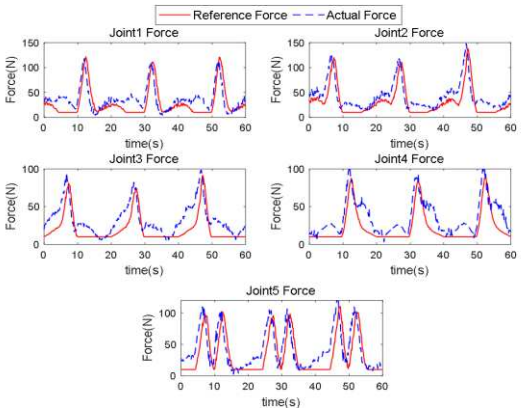

Fig. 11. Force tracking results of each PM of the ankle rehabilitation robot controlled by HFPC with participant S1, in which the desired force is obtained by the optimal force distribution method with the minimum driving force set to 10N.

TABLE IV
STATISTICAL RESULTS OF TRAJECTORY TRACKING ERRORS UNDER TWO CONTROL METHODS WITH DIFFERENT SUBJECTS

Subject	Control method	AE (degrees)			RMSE (degrees)		
		X	*Y*	*Z*	*X*	*Y*	*Z*
S1	ABS-SMC	**1.09**	0.95	0.43	1.17	1.08	0.51
	HFPC	**1.55**	1.51	0.76	1.81	1.75	0.92
S2	ABS-SMC	1.03	0.88	0.44	**1.18**	1.07	0.54
	HFPC	1.41	1.39	0.85	1.64	1.67	**1.03**
S3	ABS-SMC	0.92	**0.98**	**0.84**	1.04	**1.09**	**0.57**
	HFPC	1.76	1.31	0.78	**1.96**	1.62	0.97
S4	ABS-SMC	0.97	0.73	0.43	1.07	0.99	0.52
	HFPC	1.45	1.50	**0.88**	1.71	**1.84**	0.96
S5	ABS-SMC	0.97	0.93	0.45	1.06	1.07	0.51
	HFPC	1.48	**1.55**	0.77	1.66	1.80	0.98
Average	ABS-SMC	0.99	0.90	0.44	1.10	1.06	0.53
	HFPC	1.53	1.45	0.81	1.76	1.74	0.97

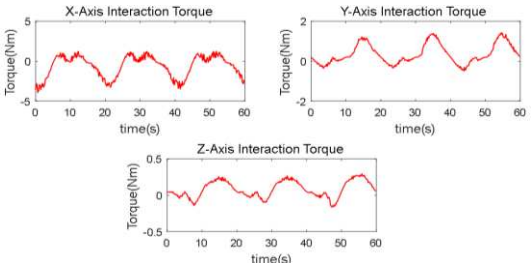

Fig. 12. Human-robot interaction measured by the six-axis force/torque sensor during robot operation with participant S1.

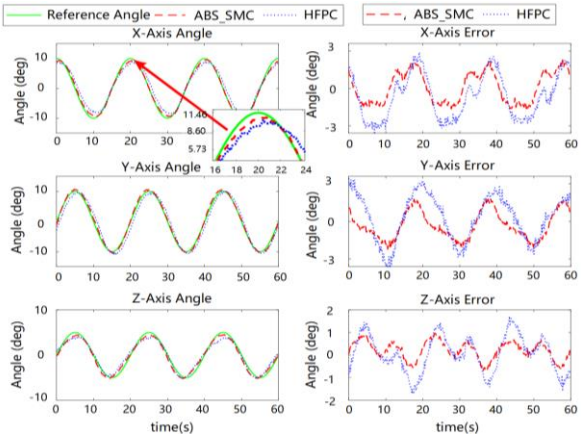

Fig. 13. Trajectory tracking results of the ankle rehabilitation controlled by ABS-SMC and HFPC with participant S1.

TABLE V
STATISTICAL RESULTS OF DRIVING FORCE TRACKING ERRORS OF EACH PM UNDER HFPC WITH DIFFERENT SUBJECTS

Subject	Error	F1	F2	F3	F4	F5
S1	AE(N)	16.381	17.401	14.617	13.905	**18.714**
	RMSE(N)	19.619	20.351	17.152	16.794	**22.560**
S2	AE (N)	12.285	15.099	13.551	13.860	17.217
	RMSE(N)	15.378	18.249	15.722	17.352	19.678
S3	AE (N)	**17.061**	13.571	11.888	**14.381**	14.663
	RMSE(N)	**20.046**	17.641	15.280	16.806	19.678
S4	AE (N)	13.054	14.365	13.443	13.995	14.753
	RMSE(N)	16.242	18.643	17.215	**17.537**	16.837
S5	AE (N)	16.563	**18.659**	**15.198**	12.670	17.304
	RMSE(N)	18.905	**20.444**	**18.706**	15.098	19.495
Average	AE (N)	15.069	15.819	13.739	13.762	16.530
	RMSE(N)	18.038	19.066	16.815	16.7179	19.650

TABLE VI
COMPARISON WITH PURE POSITION CONTROL STUDIES FOR MULTI-PM DRIVEN ROBOTS

Control strategy	Performance*	Reference
The proposed HFPC	22.07%	-
Boundary layer augmented SMC	25.2%	[9]
Advanced nonlinear PID control	29.34%	[36]
Hysteresis compensation-based control	29.42%	[37]
Robust iterative feedback tuning control	17.44%	[35]

* Maximum error percentage in total movement range

V. CONCLUSION

This paper designs a 3-DOF compliant ankle rehabilitation robot redundantly driven by PMs and cables to provide sufficient driving torque and motion range for the ankle joint. To ensure the controllability and safety of the soft redundant robot, all PMs need to be controlled in tension during the operation. An optimal force distribution method based on KKT and analytic-iterative algorithm is proposed to ensure that the force of each PM is always positive. A hierarchical force-position controller (HFPC) is proposed with an ABS-SMC position control loop and an optimal force control loop. Experimental results show that the method can ensure the tracking accuracy and keep all PMs in tension, regardless of whether the subjects are involved or not. Therefore, the safety and controllability during rehabilitation can be guaranteed by using the proposed HFPC method. Due to the PM's adjustable compliance, the future work will focus on adaptive compliance control of the ankle rehabilitation robot based on the HFPC and the dynamic relationship between PM's stiffness and nominal pressure, to adapt to personalized rehabilitation requirement.

REFERENCES

[1] S. S. Virani, A. Alonso, H. J. Aparicio, E. J. Benjamin, and C. W. Tsao, "Heart Disease and Stroke Statistics—2021 Update: A Report from the American Heart Association," *Circulation,* vol. 141, pp.132-153, 2021.

[2] J. Kim, T. Thayabaranathan, G. A. Donnan, G. Howard, and A. G. Thrift, "Global Stroke Statistics 2019," *Int J Stroke,* vol. 15, pp. 174749302090954, 2020.

[3] C. Doherty, C. Bleakley, E. Delahunt, and S. Holden, "Treatment and prevention of acute and recurrent ankle sprain: an overview of systematic reviews with meta-analysis," *Br J Sports Med,* vol. 51, pp. 113-125, 2017.

[4] R. Wittenberg and D. King, "The future incidence, prevalence and costs of stroke in the UK," *LSE Res Online Doc Econ,* 2020.

[5] D. Lubbe, E. Lakhani, J. W. Brantingham, G. F. Parkin-Smith, *et al.*, "Manipulative Therapy and Rehabilitation for Recurrent Ankle Sprain With Functional Instability: A Short-Term, Assessor-Blind, Parallel-Group Randomized Trial," *J Mani Phys Ther,* vol. 38, pp. 22-34, 2015.

[6] W. Meng, Q. Liu, Z. D. Zhou, Q. S. Ai, B. Sheng, and S. Q. Xie, "Recent development of mechanisms and control strategies for robot-assisted lower limb rehabilitation," *Mechatronics,* vol. 31, pp. 132-145, 2015.

[7] W. Meng, S. Q. Xie, Q. Liu, C. Z. Lu, and Q. S. Ai, "Robust Iterative Feedback Tuning Control of a Compliant Rehabilitation Robot for Repetitive Ankle Training," *IEEE Trans Mech,* vol. 22, pp. 173-184, 2017.

[8] G. C. Burdea, D. Cioi, A. Kale, W. E. Janes, S. A. Ross, and J. R. Engsberg, "Robotics and gaming to improve ankle strength, motor control, and function in children with cerebral palsy-A case study series," *IEEE Trans Neural Syst Rehab Eng,* vol. 21, pp. 165-173, 2013.

[9] P. K. Jamwal, S. Hussain, M. H. Ghayesh, and S. V. Rogozina, "Impedance control of an intrinsically compliant parallel ankle rehabilitation robot," *IEEE Trans Ind Electron,* vol. 63, pp. 3638-3647, 2016.

[10] M. Zhang, J. Cao, G. Zhu, Q. Miao, X. Zeng, and S. Q. Xie, "Reconfigurable workspace and torque capacity of a compliant ankle rehabilitation robot (CARR)," *Rob Autom Syst,* 2017.

[11] W. Zang, K. Zang, G. Shen, X. Li, *et al.*, "Position, Jacobian, decoupling and workspace analysis of a novel parallel manipulator with four pneumatic artificial muscles," *J Brazil Soc Mech Sci Eng,* vol. 41, 2019.

[12] X. K. Tu, J. X. Li, J. Li, C. Su, *et al.*, "Model-Based Hybrid Cooperative Control of Hip-Knee Exoskeleton and FES Induced Ankle Muscles for Gait Rehabilitation," *Int J Pattern Recogn Artif Intell,* vol. 31, 2017.

[13] S. Krishnan, A. Krishna, A. Nordin, V. Amirtham, A. M. A. Rani, and T. Rao, "Design and Fabrication of a Parallel Mechanism for Foot/Ankle Rehabilitation Therapy," *Adv Emerg Tech Eng Appl*, pp. 133-141, 2020.

[14] P. K. Jamwal, S. Q. Xie, S. Hussain, and J. G. Parsons, "An adaptive wearable parallel robot for the treatment of ankle injuries," *IEEE Trans Mech,* vol. 19, pp. 64-75, 2014.

[15] M. Zhang, A. McDaid, A. J. Veale, Y. Peng, *et al.*, "Adaptive Trajectory Tracking Control of a Parallel Ankle Rehabilitation Robot With Joint-Space Force Distribution," *IEEE Access,* vol. 7, pp. 85812-85820, 2019.

[16] J. Kwon, J.-H. Park, S. Ku, Y. Jeong, N.-J. Paik, and Y.-L. Park, "A Soft Wearable Robotic Ankle-Foot-Orthosis for Post-Stroke Patients," *IEEE Rob Autom Lett,* vol. 4, pp. 2547-2552, 2019.

[17] M. Hassan and A. Khajepour, "Analysis of bounded cable tensions in cable-actuated parallel manipulators," *IEEE Trans Rob,* vol. 27, pp. 891-900, 2011.

[18] D. B. Reynolds, D. W. Repperger, C. A. Phillips, and G. Bandry, "Modeling the dynamic characteristics of pneumatic muscle," *Ann Biomed Eng,* vol. 31, pp. 310-317, 2003.

[19] V. Jouppila, S. A. Gadsden, and A. Ellman, "Experimental comparisons of sliding mode controlled pneumatic muscle and cylinder actuators," *J Dyn Syst Meas Control,* vol. 136, pp. 044503, 2014.

[20] Q. S. Ai, C. X. Zhu, J. Zuo, W. Meng, Q. Liu, S. Q. Xie, *et al.*, "Disturbance-Estimated Adaptive Backstepping Sliding Mode Control of a Pneumatic Muscles-Driven Ankle Rehabilitation Robot," *Sensors,* vol. 18, pp. 66, 2018.
[21] N. Mostashiri, J. Dhupia, A. Verl, and W. Xu, "A Review of Research Aspects of Redundantly Actuated Parallel Robots for Enabling Further Applications," *IEEE Trans Mech,* pp. 1-12, 2018.
[22] H. Y. Wen, M. Cong, G. F. Wang, W. L. Qin, W. L. Xu, *et al.*, "Dynamics and Optimized Torque Distribution Based Force/position Hybrid Control of a 4-DOF Redundantly Actuated Parallel Robot with Two Point-contact Constraints," *Int J Control Autom Syst,* vol. 17, pp. 1293-1303, 2019.
[23] Y. Su, Y. Qiu, and L. Wang, "Optimization of redundant driving force for high-speed cable-driven parallel camera robots," *J Xidian U,* vol. 41, pp. 90-96, 2014.
[24] Y. Mao and S. K. Agrawal, "Design of a Cable-Driven Arm Exoskeleton (CAREX) for Neural Rehabilitation," *IEEE Trans Rob,* vol. 28, pp. 922-931, 2012.
[25] X. Jin, X. Cui, S. K. Agrawal, "Design of a Cable-driven Active Leg Exoskeleton (C-ALEX) and Gait Training Experiments with Human Subjects," *IEEE Int Conf Rob Autom*, pp. 5578-5583, 2015.
[26] R. Hidayah, L. Bishop, X. Jin, S. Chamarthy, J. Stein, and S. K. Agrawal, "Gait Adaptation Using a Cable-Driven Active Leg Exoskeleton (C-ALEX) With Post-Stroke Participants," *IEEE Trans Neural Syst Rehab Eng,* vol. 28, pp. 1984-1993, 2020.
[27] M. Hassan and A. Khajepour, "Optimization of actuator forces in cable-based parallel manipulators using convex analysis," *IEEE Trans Rob,* vol. 24, pp. 736-740, 2008.
[28] H. Yuan, E. Courteille, and D. Deblaise, "Force distribution with pose-dependent force boundaries for redundantly actuated cable-driven parallel robots," *J Mech Rob,* vol. 8, pp. 041004, 2016.
[29] W. Meng, C. Zhu, J. Zuo, Q. Ai, and S. Q. Xie, "Design and Modelling of a Compliant Ankle Rehabilitation Robot Redundantly Driven by Pneumatic Muscles," *IEEE/ASME Int Conf Adv Intell Mech (AIM)*, 2019.
[30] H. D. Taghirad and Y. B. Bedoustani, "An analytic-iterative redundancy resolution scheme for cable-driven redundant parallel manipulators," *IEEE Trans Rob,* vol. 27, pp. 1137-1143, 2011.
[31] F. Sabahi, M. A. Khosravi, and H. D. Taghirad, "Implementation of Analytic Iterative Redundancy resolution technique on KNTU cable robot," *Int Conf Rob Mech (ICRoM)*, pp. 690-694, 2014.
[32] A. Pott, "On the Limitations on the Lower and Upper Tensions for Cable-Driven Parallel Robots," *Adv Rob Kinem,* pp. 243-251, 2014.
[33] S. A. Khalilpour, R. Khorrambakht, H. D. Taghirad, and P. Cardou, "Robust cascade control of a deployable cable- driven robot," *Mech Syst Signal Process,* vol. 127, pp. 513-530, 2019.
[34] I. Chawla, P. M. Pathak, L. Notash, A. K. Samantaray, Q. Li, and U. K. Sharma, "Effect of selection criterion on the kineto-static solution of a redundant cable-driven parallel robot considering cable mass and elasticity," *Mech Mach Theory,* vol. 156, pp. 147-154, 2021.
[35] W. Meng, S. Q. Xie, Q. Liu, C. Z. Lu, and Q. Ai, "Robust Iterative Feedback Tuning Control of a Compliant Rehabilitation Robot for Repetitive Ankle Training," *IEEE Trans Mech,* vol. 22, pp. 173-184, 2017.
[36] G. Andrikopoulos, G. Nikolakopoulos, and S. Manesis, "Motion control of a novel robotic wrist exoskeleton via pneumatic muscle actuators," *Emerg Tech Fact Autom*, pp. 1-8, 2015.
[37] S. Xie, G. Ren, J. Xiong, and Y. Lu, "A Trajectory Tracking Control of a Robot Actuated With Pneumatic Artificial Muscles Based on Hysteresis Compensation," *IEEE Access,* vol. 8, pp. 80964-80977, 2020.